E18-2007-91

M. Rajcan[1,2], A. G. Molokanov[1], M. Mumot[1,3]

SIMULATIONS OF PROTON BEAM DEPTH-DOSE DISTRIBUTIONS

[1]Joint Institute for Nuclear Research, Dubna
[2]Slovak Institute of Metrology, Center for Ionizing Radiation, Bratislava
[3]Department of Medical Physic, Great Poland Cancer Centre, Poznań

Райчан М., Молоканов А. Г., Мумот М. E18-2007-91
Моделирование глубинных дозных распределений протонного пучка

Протонные пучки успешно применяются в радиотерапии. Правильный выбор параметров пучка позволяет уменьшить воздействие радиации на окружающие здоровые ткани. В работе рассматривается пассивная техника формирования параметров протонного пучка. Протонный пучок проходит через систему формирования, которая состоит из рассеивателей, замедлителей пучка, дрейфовых промежутков и коллиматоров. С целью моделирования прохождения протонного пучка через эту систему была разработана новая Монте-Карло компьютерная программа Track. Программа Track позволяет предсказать параметры протонного пучка после прохождения через элементы системы формирования и помогает их оптимизировать. Track вычисляет профили пучка, создает диаграммы эмиттанса для определенной конфигурации системы формирования и моделирует глубинные дозные распределения протонного пучка в водном фантоме. Кроме того, дополнительно вычисляются потери пучка в отдельных элементах системы.

В работе представлена физическая модель вычислений транспортировки пучка и алгоритм, примененный в программе Track. Результаты моделирования глубинных дозных распределений протонного пучка в водном фантоме сравниваются с экспериментальными данными и с симуляциями по программе FLUKA. Исследовалась точность результатов моделирования и вычислительное время программы Track.

Работа выполнена в Лаборатории ядерных проблем им. В. П. Джелепова ОИЯИ.

Сообщение Объединенного института ядерных исследований. Дубна, 2007

Rajcan M., Molokanov A. G., Mumot M. E18-2007-91
Simulations of Proton Beam Depth-Dose Distributions

Proton beams are successfully used in radiotherapy. A correct modification of beam parameters enables to spare normal surrounding tissues from radiation action. Our work is focused on passive beam-shaping techniques, which are used to modify the proton beam properties. The beam passes through the scattering system, which consists of scattering materials, energy degraders, drift spaces and collimators. In order to model the proton beam transport through the scattering system, the new Monte Carlo (MC) computer code Track has been developed. The code Track can predict output proton beam parameters modulated by various system adjustments and helps to optimize them. It calculates a beam profile, creates beam emittance diagram at a specified position of the system and predicts proton beam depth-dose distribution in a water phantom. In addition it calculates beam losses on individual components.

We present a physical model of the beam transport calculations and algorithm implemented in a code Track. We compared the Track code calculations of depth-dose distributions in water phantom with experimental data and with a set of MC calculations in the FLUKA code. The accuracy of simulation results and calculation time in Track code are observed.

The investigation has been performed at the Dzhelepov Laboratory of Nuclear Problems, JINR.

Communication of the Joint Institute for Nuclear Research. Dubna, 2007

INTRODUCTION

Increasing number of proton therapy centers indicates to the worldwide interest in exploiting and improving proton therapy techniques also in the future [1]. Proton beams are successfully used for treatment cancer diseases. They have advantageous physical and radiobiological properties in their use in radiotherapy [2]. Minimal lateral diffusion, energy scattering and deposition of maximum energy at the end of proton range allow delivering a high dose rate to the target volume. Conformal radiotherapy requires accurate and precise geometric targeting of the tumor. A correct modification of beam parameters enables to spare normal surrounding tissues from radiation action. In accordance with firm therapy needs, every treated lesion demands for individual beam preparation.

Our work is focused on passive beam-shaping techniques, which are used to modify the proton beam properties [3, 4]. The beam passes through the appropriate system of scattering materials, energy degraders, drift spaces and collimators. This system will be referred as a scattering system. There are relatively good base of established Monte Carlo (MC) codes to solve such proton transport tasks, namely, FLUKA [5], Geant4 [6], MCNPX [7] or SHIELD-HIT [8]. Each offers a number of different physical models, radiation transport algorithms, which potentially leads to significantly different predictions of results [9]. These codes can solve a wide range of problems, however the main difficulty remains in their long computation time. The motivation to develop new specialized proton transport codes speeding computations up along with keeping sufficient accuracy can be seen elsewhere [10–14].

In order to model the proton beam transport through the scattering system, the new MC computer code Track has been developed. The code Track can predict output beam parameters modulated by various system adjustments and helps to optimize them. It calculates a beam profile, creates beam emittance diagram at a specified position of the system and predicts proton beam depth-dose distribution in a water phantom. In addition, it calculates beam losses on individual components.

This paper presents a physical model implemented in a proton transport code called Track. We compared preliminary calculations in Track with experimental results and with a set of MC calculations in FLUKA code. The accuracy of simulation results and calculation time in Track code are observed.

1. METHODS

1.1. Input Beam. In the code Track the proton is characterized by its positional coordinates (x, y, z), direction coordinates (x', y', z') and kinetic energy T. Primary beam direction is in the y axis. The beam can be defined by emittance diagram parameters in the planes (x, x') and (z, z') separately [15]. The emittance diagram of the beam is randomly filled in by a default number of particles with the Gaussian beam profile. A collimated input beam models circular or rectangular profile with the homogeneous proton distribution. The input beam energy spectrum has the Gaussian form with the specified mean value and the standard deviation. Additionally, different energy spectra can be modeled, if their distributions are available.

1.2. Scattering System. The scattering system consists of various materials placed on the beam line, namely, scattering foils, energy degraders, energy modulators, collimators, drift spaces, boluses, etc [16]. Scattering elements are defined by their position, material characteristics (effective charge, effective atomic mass and density) and geometric shape. Total stopping powers calculated by computer code PSTAR [17] were used to evaluate material slowing down properties in the prepared form of the proton range-energy tables.

The scattering element should be described by the sequence of plane parallel layers where each of them consists of one material. To increase the calculation speed the proton passes through the scattering layer in a one single step. The proton undergoes angular scattering and energy straggling in the simulation's transport model. In the water phantom additionally elastic and inelastic scatterings, between proton and oxygen nucleus O16, are simulated. In an arbitrary position of the scattering system the Track code can register proton positions, angular deflections and energies. This information is essential to create beam emittance diagram, beam profile and proton energy spectra.

The code Track calculates at the beginning of a simulation output angular and energy distributions necessary for the proton transport through the scattering layer. Distributions are evaluated for incident protons of this kinetic energy sequence:

$$T_n = 300 \cdot (1 - 0.01)^{n-1} \quad [\mathrm{MeV}] \tag{1}$$

The sequence (1) is decreasing with a difference of one per cent between neighboring proton kinetic energies, where the integer n goes from 1 to $n_{\max} = 638$, which define minimal kinetic energy $T_{\min} \approx 0.5$ MeV of a transported proton. The transport of proton with kinetic energy less than $T_{\min}$ ends. Each proton kinetic energy T_p from 0.5 to 300 MeV can be assigned to a specific energy interval:

$$T_{n+1} \leqslant T_p \leqslant T_n \tag{2}$$

Kinetic energies T_{n+1} and T_n belong to the sequence (1).

1.3. Angular Scattering. The proton traversing through the material undergoes a significantly large amount of scatterings with atomic electrons and nuclei. This effect is called multiple Coulomb scattering. The angular scattering simulation is based on the Molière multiple scattering theory [18–21]. First three terms of Molière distribution are considered to calculate the angular distributions. Scattering layer with a relativeey large thickness t is automatically divided into shorter thicknesses, whose values are produced by geometric series [22]:

$$t_i = kR\,(1-k)^{i-1}\,, \tag{3}$$

where R is proton range in the material at the incident kinetic energy, i is integer number from 1 to maximum 8. Constant $k = 0.375$ guarantees the maximum splitting into eight shorter layers, while the Molière theory is still valid. Characteristic single scattering angle and effective value of screening angle are calculated by numerical integration through all the layers of thicknesses t_i [22].

The code Track calculates inverse cumulative distributions (ICD) of proton angular deflections $\theta\,(u)$ for all the layers in the scattering system as functions of cumulative probability u. Consequently the output is saved in the tables. Each table contains 1000 values with a constant step of cumulative probability u. By picking a uniform random number u between 0 and 1, angular deflection is sampled as a result of the linear interpolation from the tabulated data [23]. This approach creates sharp ragged continuous probability distribution function, especially for small angular deflections. It may lead to broken beam profile in the central part at distance from the acting scatterer. Therefore, the first ten of tabulated small deflections are approximated by a function

$$\theta\,(u) = \theta_0\left(1-(1-4u)^{1/2}\right)^{1/2}, \tag{4}$$

where θ_0 is parameter calculated by least squares method. If one considers the following approximation of probability distribution $p\,(\theta)$ for small deflections θ

$$p\,(\theta) \approx \frac{\theta}{\theta_0^2}\exp\left(-\frac{\theta}{\theta_0^2}\right), \tag{5}$$

then the cumulative distribution $c\,(\theta)$ can be expressed as

$$c\,(\theta) \approx \frac{\theta^2}{2\theta_0^2} - \frac{\theta^4}{4\theta_0^4}. \tag{6}$$

The inversion of Eq. (6) leads to expression (4). This expression is used to sample the deflection angle $\theta\,(u)$ for random number u from interval $[0,\,0.01]$. The sampled deflections of small angles then produce smooth continuous distribution.

1.4. Energy Straggling. The fluctuations of proton energy loss in matter are simulated in accordance with the Vavilov theory [24, 25]. The analytical Vavilov distribution function was numerically analyzed for the purpose of calculations of energy straggling distributions [26]. The code Track calculates ICD of kinetic energy for protons leaving the target layers. The method to store ICD and sample the kinetic energy is the same as discussed in Subsec. 1.3. with angular deflections.

1.5. Kinetic Energy and Angular Deflection of a Scattered Proton. The path length of protons in the scattering layer is approximately the same as the layer thickness t, if protons incident perpendicularly and the layer are thin with respect to the proton range. Proton entering into the layer with deflection from normal direction travels the larger path length because of geometrical reason. One can assume that the main part of protons, transported through the scattering system, has angular deflection less than 0.43 rad from the beam axis. This value corresponds to approximately 10% increase of the path length in the layer. Then the majority of protons travel path length t_p through the scattering layer

$$t < t_p < t_{+10\%}, \tag{7}$$

where path lengths t and $t_{+10\%}$ correspond to proton angular deflections from the beam axis of 0 and 0.43 rad, respectively. The code Track calculates also ICD functions for larger proton path length $t_{+10\%}$ in the layer. Angular $\theta\,(u, T_p, t_p)$ and energy $T\,(u, T_p, t_p)$ ICD functions depend approximately linear on the proton kinetic energy T_p and path length t_p within intervals (2) and (7), respectively, for generated random number u. The error from this linearity is smaller than 1%. As discussed before, variable u represents random number from uniform interval $[0, 1]$.

The algorithm to sample new angular deflection and kinetic energy of transported proton through the layer consists of these steps:

1. Specification of energies T_n and T_{n+1} which satisfy the condition (2).
2. Generation of two random numbers u_θ and u_T from uniform interval $[0, 1]$. Calculation of angles $\theta\,(u_\theta, T_n, t)$, $\theta\,(u_\theta, T_{n+1}, t)$, $\theta\,(u_\theta, T_n, t_{+10\%})$, $\theta\,(u_\theta, T_{n+1}, t_{+10\%})$ and energies $T\,(u_T, T_n, t)$, $T\,(u_T, T_{n+1}, t)$, $T\,(u_T, T_n, t_{+10\%})$, $T\,(u_T, T_{n+1}, t_{+10\%})$ from calculated ICD tables.
3. Proton deflection angle $\theta\,(u_\theta, T_p, t_p)$ and kinetic energy $T\,(u_T, T_p, t_p)$ after scattering are calculated by linear interpolation of results from the previous step 2.

Scattered proton is deflected against initial direction about angle $\theta\,(u_\theta, T_p, t_p)$ and can rotate around with angle β, which is sampled from uniform interval $[0, 2\,\pi]$. Appropriate rotational transformations are applied to calculate the new proton direction.

1.6. The Water Phantom. Transport of protons in water phantom differs from that in the scattering layers. Protons undergo elastic and inelastic scatterings on oxygen nuclei in the simulation. Interaction probability represents the prepared cross section table. This depends on incident proton kinetic energy. Inelastic interacted protons and some with kinetic energy less than 0.5 MeV are stopped. Secondary protons interact as well as primary. The drift length of proton in simulation depends on its incident kinetic energy T_p. For energies (1) the corresponding step lengths $D(T_n)$, on which the mean proton energy loss represents 1%, are calculated. Linear interpolation is used to calculate the drift $D(T_p)$ from two values $D(T_n)$ and $D(T_{n+1})$ according to (2). Angular $\theta(u_\theta, T_n)$ and kinetic energy $T(u_T, T_n)$ ICD functions described in Subsecs. 1.3. and 1.4 are calculated for proton kinetic energies (1) with corresponding drift in water $D(T_n)$. Then these are functions of the two variables, i. e., random number and incident kinetic energy, which are coupled with drift length. The new angular deflection $\theta(u_\theta, T_p)$ and kinetic energy $T(u_T, T_p)$ are calculated from two values $\theta(u_\theta, T_n)$, $\theta(u_\theta, T_{n+1})$ and $T(u_T, T_n)$, $T(u_T, T_{n+1})$, respectively, using linear interpolations

$$\theta(u_\theta, T_p) = (T_p - T_{n+1}) \frac{\theta(u_\theta, T_n) - \theta(u_\theta, T_{n+1})}{T_n - T_{n+1}} + \theta(u_\theta, T_{n+1}), \quad (8)$$

$$T(u_T, T_p) = (T_p - T_{n+1}) \frac{T(u_T, T_n) - T(u_T, T_{n+1})}{T_n - T_{n+1}} + T(u_T, T_{n+1}). \quad (9)$$

The proton drift $D(T_P)$ is divided into two parts

$$D_1(u, T_p) = uD(T_p), \quad (10)$$

$$D_2(u, T_p) = (1-u)D(T_p), \quad (11)$$

where random number u is within uniform interval $[0, 1]$. The proton is transported first along the step D_1 and its kinetic energy loss ΔT_1 is proportional to D_1

$$\Delta T_1 = -\frac{D_1}{D(T_p)}(T_p - T(u_T, T_p)). \quad (12)$$

At this position the new direction of proton is calculated with respect to deflection angle $\theta(u_p, T_p)$. Elastic, inelastic or both interactions can occur between proton and oxygen nucleus. In case no inelastic interaction occurs, proton is transported to the end of drift $D(T_P)$ with step D_2. Then kinetic energy loss ΔT_2 of proton is proportional to D_2

$$\Delta T_2 = -\frac{D_2}{D(T_p)}(T_p - T(u_T, T_p)). \quad (13)$$

The proton dose is calculated in the region of cylindrical shape. Each cylinder «detector» with defined radius and height is situated one after the other so that its axis is identical with beam axis. The dose released by a proton in the specific cylinder is proportional to the length of one straight proton track D inside this cylinder

$$\text{Dose} = \frac{D}{D\left(T_p\right)} \frac{T_p - T\left(u_T, T_p\right)}{M}, \tag{14}$$

where M is a mass of cylindrical detector.

1.7. Inelastic Interaction. Transport of primary proton after inelastic interaction ends. Its kinetic energy is released to secondary particles. The code Track calculates transport of secondary protons only. The probability of creation 0, 1, 2 or 3 secondary protons is calculated in accordance with multiplicity evaluated in ENDF-VI file [27] and kinetic energy of incident proton. The energy transferred to heavier charged particles (heavier than a proton) because their short range is deposited at the site of interaction. Long-range particles (neutron, gamma) interact far from the proton track. They are assumed to leave the scoring geometry without any energy deposition [11]. The energy fractions transferred to these different types of particles are evaluated using ICRU 63 data [28]. The energy of secondary protons is sampled from the emission spectra integrated over all angles, which are evaluated in ENDF-VI files. Input library of the code Track contains ICD functions of secondary proton emission spectra. The angular deflections of secondary protons after interaction are calculated by using the Kalbach-Mann systematic [29, 30].

1.8. Elastic Interaction. The angular deflection of a proton after elastic interaction on oxygen O16 nucleus is sampled from ICD functions, which are saved in tables. Calculation of these ICD functions is based on inversion of the integral of the net elastic scattering cross section

$$\sigma_e(\mu, E) = \sigma_{NI}(E) P_{NI}(\mu, E) + \sigma_C(\mu, E), \tag{15}$$

where μ is cosine of the scattering angle in the center of mass system, E is kinetic energy of the incident proton in the laboratory system, $\sigma_{NI}(E)$ is integral of nuclear plus interference components of the elastic scattering cross section, $P_{NI}(\mu, E)$ is nuclear plus interference cross section, $\sigma_C(\mu, E)$ is differential Coulomb scattering cross section evaluated in [27]. The functions $\sigma_{NI}(E)$ and $P_{NI}(\mu, E)$ are evaluated in ENDF-VI file. Energy of scattered proton results from the kinematical conditions of elastic scattering. Energy transferred to oxygen is deposited at the site of interaction.

2. RESULTS

On the proton therapeutical beam of the DLNP, JINR Dubna phasotron, depth-dose distributions in water phantom were measured. Influence of forming

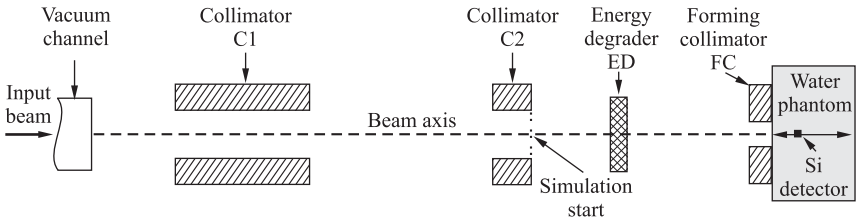

Fig. 1. Scheme of the experimental set-up. Collimators C1 and C2 absorb scattered protons above the useful field. Energy degrader ED slows down the proton energy. Collimator FC forms proton field incident to the water phantom

collimator dimensions on shape of the Bragg curve was observed. The material of these collimators was copper and Cerrobend (alloy of Pb — 25%, Sn — 12.5%, Bi — 50% and Cd — 12.5%). The dose was measured by silicon diode within water phantom along the beam axis. The layout of experimental set-up is shown in Fig. 1. The collimator C2 defines the input beam profile used in simulation. The same conditions of the proton beam transport were simulated with the code Track. The simulation starts at the output of the the collimator C2, where the model of input beam is defined. Acting of air was not considered in this study, because of its low effect on beam degrading and scattering.

The measured depth-dose distribution cannot be reproduced by simulation with proton beam with Gaussian form of the energy spectrum only. The model of real energy spectrum is then determined by the following technique. The depth-dose distribution obtained experimentally in the water phantom was fitted by function

$$\mathrm{Dose}(t_w) = \sum_i w_i \cdot \mathrm{Dose}_i\,(t_w)\,, \tag{16}$$

where $\mathrm{Dose}(t_w)$ is dose distribution depending on the depth t_w in water, w_i is wanted parameter for ith simulated distribution $\mathrm{Dose}_i\,(t_w)$ of monoenergetic proton beam with energy

$$T_i = 70 + 2i \quad [\mathrm{MeV}] \tag{17}$$

for integer i from 0 to 58. The set of distributions $\mathrm{Dose}_i\,(t_w)$ was calculated in the Track code. Consequently by iterative process the suitable values of w_i were found to match dose distribution (16) with that obtained experimentally. The relation between parameters w_i and corresponding energies T_i was approximated by two functions (18), (19). These functions were associated with energy spectrum of input beam (see Fig. 2). Their integral is normalized to unity. The energy degrader ED stops protons with kinetic energy less than approximately 70 MeV, therefore these are not considered in simulated spectra.

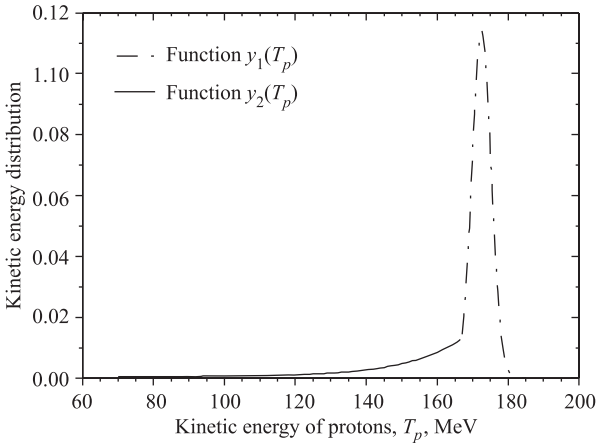

Fig. 2. Kinetic energy spectra of input proton beam used in simulations

The first function has Gaussian form with a mean value of 172.5 MeV and a standard deviation of 2.7 MeV (18). Second function (19) has a form of exponential growth.

$$y_1\,(T_p) = 0.114\,\exp\left(-0.5(T_p - 172.5)^2/2.7^2\right);\; 167 \leqslant T_p < 186\,\mathrm{MeV}, \quad (18)$$

$$y_2\,(T_p) = 5 \cdot 10^{-4} + 2.7 \cdot 10^{-7}\exp\,(T_p/15.54)\,;\; 70 \leqslant T_p < 167\,\mathrm{MeV}. \quad (19)$$

Presented model of energy spectrum is not certainly accurate, but is sufficient to describe real proton beam in our simulations. Low energy part «tail» in this spectrum can be explained as follows. Proton beam is broad enough to hit walls of vacuum channel and first collimator before entering the therapeutical room. Some protons are slowed down in these walls and scattered back to the beam axis.

Figure 3 shows depth-dose distributions behind Cerrobend collimators. The lengths L of collimators FC were approximately the same. In Fig. 4 one can see different dose distributions behind copper collimators with the same aperture D and various lengths L. The lower area of the beam is transmitted through the longer collimator. Then the Bragg peak is lower.

The energy degrader ED additionally scatters protons to the collimator walls. The reduced diameter of collimator FC causes drop of Bragg peak to a lower level. In the case of narrow beam, the number of protons scattered out from the beam axis in phantom is lower than the number of protons incoming from the beam border. Entrance beam dose increase by protons slowed down in the collimator

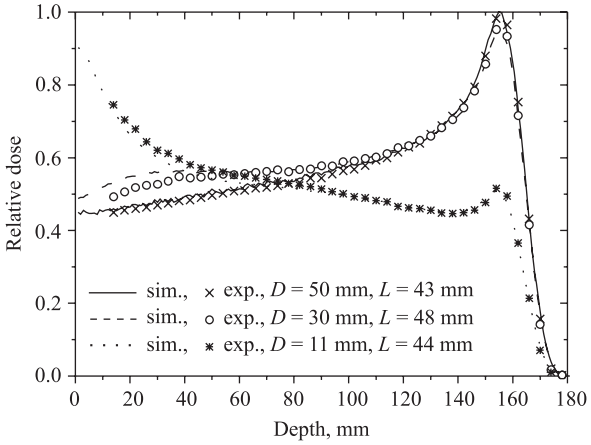

Fig. 3. Depth-dose distributions of proton beam in water phantom behind Cerrobend collimators of various aperture D and length L. Symbols represent experimental data, lines denote simulations

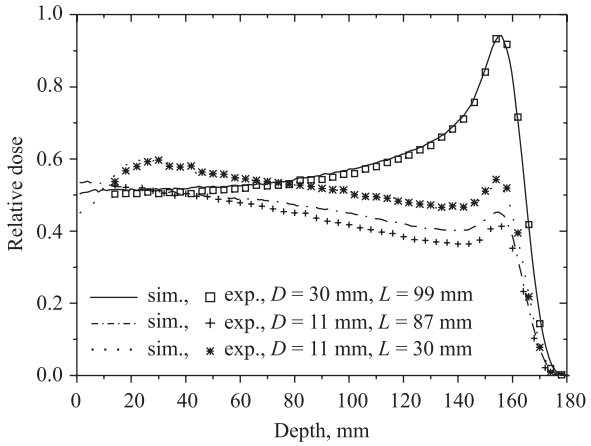

Fig. 4. Depth-dose distributions of proton beam in water phantom behind copper collimators of various aperture D and length L. Symbols represent experimental data, lines denote simulations

FC walls. The contribution of slowed protons is lower behind collimator FC with bigger aperture.

Additional simulations were done in Track and FLUKA codes. Parallel monoenergetic proton beam incidents to the water phantom. Beam profile was circular with diameter of 20 mm. The dose was calculated in the slabs oriented perpendicular to the incident beam, having an area of 100 cm^2 and thickness of 0.1 mm. The detected area is broad enough compared to the incident beam. This

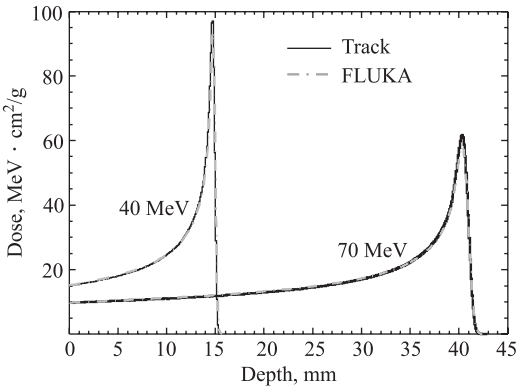

Fig. 5. Depth-dose distributions of monoenergetic proton beams with incident kinetic energies of 40 and 70 MeV in water phantom. Simulations are performed with the Track and FLUKA codes

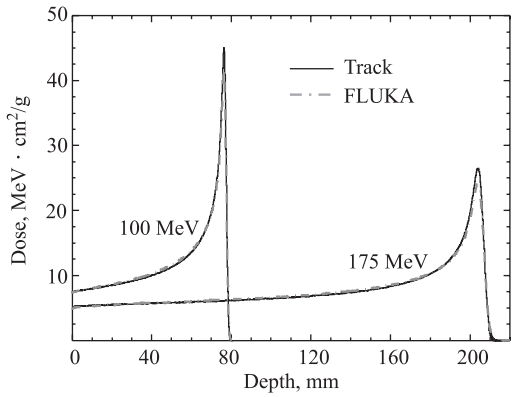

Fig. 6. Depth-dose distributions of monoenergetic proton beams with incident kinetic energies of 100 and 175 MeV in water phantom. Simulations are performed with the Track and FLUKA codes

absorbs all the transported protons. Only long-range particles (neutron, gamma) in FLUKA simulations can leave this scoring geometry. Figures 5, 6 show simulated depth-dose distributions of monoenergetic proton beams with energies of (40, 70) and (100, 175) MeV, respectively. The detailed trends of simulated depth-dose distributions in the Bragg peak region for these two codes are shown in Fig. 7.

The simulation with the Track code is approximately 12 times faster compared to the FLUKA code. The calculation time was measured on the same computer with identical simulation conditions. Althogh the word «identical» is not fully correct, because the FLUKA code additionally provides the detailed transport of

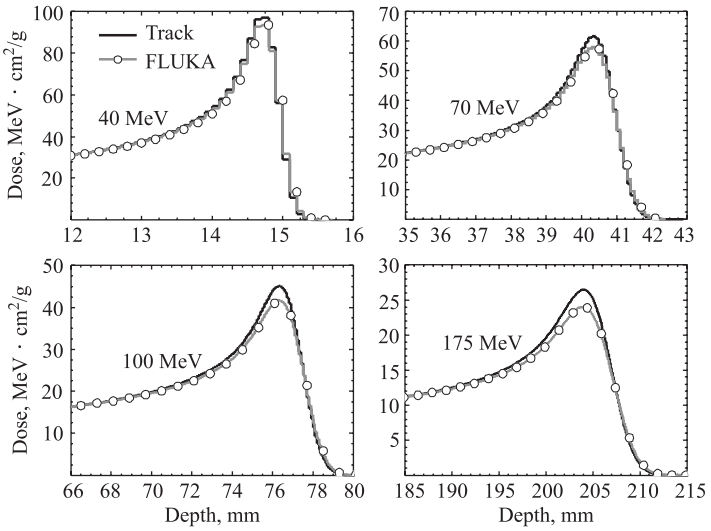

Fig. 7. Detailed shapes of simulated depth-dose distributions in the Bragg peak region. Simulations are performed with the Track and FLUKA codes for monoenergetic 40, 70, 100 and 175 MeV proton beams

secondary particles such as neutrons, gamma and charged particles heavier than proton, what increases the calculation time.

CONCLUSIONS

Our new Track Monte Carlo code showed very good agreement with experimental data. From obtained results we can conclude that it simulates accurately enough all the scattering system: scattering materials, degraders, collimators, drift spaces, and also water phantom.

We observed effect of scattered protons for collimator with different apertures, lengths and materials. The collimator effect is bigger for collimators with lower aperture. Track code allowed us to predict this effect as well as its quantitatively dose contribution.

Comparison of dose distributions calculated with Track and FLUKA MC codes indicated that Track code overestimates the FLUKA results up to about 10% in the Bragg peak region. It can be connected with different physical approach used in the codes. The FLUKA code transports also neutrons, gamma and heavy ions, created in inelastic interactions and Track does not. The big

advantage of Track code comparing with FLUKA is the time of calculating: Track is approximately 12 times faster compared to the FLUKA code.

REFERENCES

1. *Dosanjh M., Hoffmann H. F., Magrin G.* // Nucl. Instr. Meth. A. 2007. V. 571. P. 191–194.
2. *Wilson R. R.* // Radiology. 1946. V. 47. P. 487–491.
3. *Koehler A. M., Schneider R. J., Sisterson J. M.* // Med. Phys. 1977. V. 4. P. 297–301.
4. *Chu W. T., Ludewigt B. A., Renner T. R.* // Rev. Sci. Instrum. 1993. V. 64. P. 2055–2122.
5. *Fasso' A., Ferrari A., Ranft J., Sala P. R.* FLUKA: a Multi-Particle Transport Code. CERN-2005-10, INFN/TC_05/11, SLAC-R-773, 2005.
6. *Allison J. et al.* // Trans. Nucl. Sci. 2006. V. 53, Issue 1. P. 270–278.
7. MCNPX User's Manual, Version 2.4.0. LA-CP-02-408 / Ed. Waters L. S. Los Alamos National Laboratory, 2002. http://mcnpx.lanl.gov.
8. *Gudowska I. et al.* // Phys. Med. Biol. 2004. V. 49. P. 1933–1958.
9. *Baker C. et al.* // Nucl. Instr. Meth. A. 2006. V. 562. P. 1005–1008.
10. *Berger M. J.* Proton Monte Carlo Transport Program PTRAN. National Institute for Standards and Technology. Report NISTIR 5113. Gaithersburg: NIST, 1993.
11. *Medin J., Andreo P.* PETRA–Monte Carlo Simulation of Proton and Electron Transport in Water. Internal Report MSF 1997-01. Department of Medical Radiation Physics, Stockholm University, 1997.
12. *Fippel M., Soukup M.* // Med. Phys. 2004. V. 31. P. 2263–2273.
13. *Palmans H.* McPTRAN.CAVITY and McPTRAN.RZ, Monte Carlo Codes for the Simulation of Proton Beams and Calculation of Proton Detector Perturbation Factors. The Monte Carlo Method: Versatility Unbounded in a Dynamic Computing World. (Illinois: American Nuclear Society, USA) ISBN 0-89448-695-0.2 005.
14. *Ilic R. D. et al.* // Phys. Med. Biol. 2005. V. 50. P. 1011–1017.
15. *Wiedemann H.* Particle Accelerator Physics I. Berlin: Springer-Verlag, 1993.
16. *Chu W. T., Ludewigt B. A., Renner T. R.* // Rev. Sci. Instrum. 1993. V. 64. P. 2055–2122.

17. *Berger M. J.* ESTAR, PSTAR, and ASTAR: Computer Programs for Calculating Stopping Power and Range Tables for Electrons, Protons, and Helium Ions, NISTIR 4999, Gaithersburg National Institute of Standards and Technology MD, 1993.

18. *Molière G. Z.* // Z. Naturfoschg. 1948. Bd. 3a. S. 78–97.

19. *Bethe H. A.* // Phys. Rev. 1953. V. 89. P. 1256–1266.

20. *Fano U.* // Phys. Rev. 1954. V. 93. P. 117–120.

21. *Scott W. T.* // Rev. Mod. Phys. 1963. V. 35. P. 231–313.

22. *Gottschalk B. et al.* // Nucl. Instr. Meth. B. 1993. V. 74. P. 467–490.

23. *Yao W. M. et al.* // J. Phys. G. 2006. V. 33, Issue 1. (http://pdg.lbl.gov).

24. *Vavilov P. V.* // J. Exp. Theor. Phys. 1957. V. 32. P. 920–923.

25. *Rotondi A., Montagna P.* // Nucl. Instr. Meth. B. 1990. V. 74. P. 215–223.

26. *Rajcan M.* JINR Preprint P18-2006-44. Dubna, 2006.

27. *Herman M.* ENDF-102 Data Formats and Procedures for the Evaluated Nuclear Data File ENDF/B-VI and ENDF/B-VII. Report BNL-NCS-44945-05-Rev. Brookhaven National Laboratory, National Nuclear Data Center, Upton, NY, USA, 2005.

28. Nuclear Data for Neutron and Proton Radiotherapy and for Radiation Protection. ICRU Report 63. ICRU, 2000.

29. *Kalbach C., Mann F. M.* // Phys. Rev. C. 1981. V. 23. P. 112–123.

30. *Kalbach C.* // Phys. Rev. C. 1988. V. 37. P. 2350–2369.

Received on June 18, 2007.

Редактор *В. В. Булатова*

Подписано в печать 5.10.2007.
Формат 60 × 90/16. Бумага офсетная. Печать офсетная.
Усл. печ. л. 1,00. Уч.-изд. л. 1,42. Тираж 260 экз. Заказ № 55915.

Издательский отдел Объединенного института ядерных исследований
141980, г. Дубна, Московская обл., ул. Жолио-Кюри, 6.
E-mail: publish@jinr.ru
www.jinr.ru/publish/